



HAL
open science

Molecular Analysis of Nitrogen Containing Compounds in Vacuum Gas Oils Hydrodenitrogenation by(Esi+/-)-FTICR-MS

Polina Mikhaylova, Luis P. de Oliveira, Isabelle Merdrignac, Alexandra
Berlioz-Barbier, Marouan Nemri, Pierre Giusti, Gerhard Pirngruber

► **To cite this version:**

Polina Mikhaylova, Luis P. de Oliveira, Isabelle Merdrignac, Alexandra Berlioz-Barbier, Marouan Nemri, et al.. Molecular Analysis of Nitrogen Containing Compounds in Vacuum Gas Oils Hydrodenitrogenation by(Esi+/-)-FTICR-MS. Fuel, 2022, 323, pp.124302. 10.1016/j.fuel.2022.124302 . hal-03660667

HAL Id: hal-03660667

<https://ifp.hal.science/hal-03660667v1>

Submitted on 6 May 2022

HAL is a multi-disciplinary open access archive for the deposit and dissemination of scientific research documents, whether they are published or not. The documents may come from teaching and research institutions in France or abroad, or from public or private research centers.

L'archive ouverte pluridisciplinaire **HAL**, est destinée au dépôt et à la diffusion de documents scientifiques de niveau recherche, publiés ou non, émanant des établissements d'enseignement et de recherche français ou étrangers, des laboratoires publics ou privés.

1 Molecular analysis of nitrogen-containing compounds in 2 vacuum gas oils hydrodenitrogenation by (ESI+/-)-FTICR-MS

3 Polina Mikhaylova^a, Luis P. de Oliveira^a, Isabelle Merdrignac^a, Alexandra Berlioz-Barbier^a,
4 Marouan Nemri^b, Pierre Giusti^{b,c}, Gerhard D. Pirngruber^{a,*}

5 ^a*IFP Energies nouvelles, Rond-point de l'échangeur de Solaize, BP 3, 69360 Solaize, France*

6 ^b*TRTG - TotalEnergies Research & Technology Gonfreville, Carrefour n° 4, BP 27, 76700 Harfleur,*
7 *France*

8 ^c*International Joint Laboratory–iC2MC: Complex Matrices Molecular Characterization, TRTG*
9 *Refining and Chemicals, TotalEnergies, 76700 Harfleur, France*

10 ABSTRACT: This paper is a part of a study on reactivity descriptors in vacuum gas oil
11 hydrotreatment (VGO HDT). It aims to understand the differences in feeds of various process
12 origins and the corresponding hydrotreated effluents on a molecular level. Four different vacuum
13 gas oils were hydrotreated over a sulfided $NiMo/Al_2O_3$ catalyst at a wide range of temperatures
14 and residence times in order to collect HDT effluents at a broad range of hydrodenitrogenation
15 (HDN) conversions. Vacuum gas oils and HDT effluents have been analyzed by Fourier transform
16 ion cyclotron resonance mass spectrometry (FTICR-MS) in positive ESI(+) and negative ESI(-)
17 electrospray ionization modes to characterize the basic and neutral nitrogen-containing species and
18 the subtleties of HDT transformations depending on the feedstock type.

19 *Keywords:* vacuum gas oil, hydrotreatment, FTICR-MS

Abbreviations: ESI, electrospray ionization; FTICR-MS, Fourier transform ion cyclotron resonance mass spectrometry; VGO, vacuum gas oil; HDT, hydrotreatment; HDN, hydrodenitrogenation; SR VGO, straight-run vacuum gas oil; HCGO, heavy coker gas oil; HVGO, hydroprocessed vacuum gas oil; GO, gas oil; DMDS, dimethyl disulfide; DBE, double bond equivalent; nC, number of carbon atoms; LHSV, liquid hourly space velocity; AR, atmospheric residue.

*Corresponding author.

E-mail address: gerhard.pirngruber@ifpen.fr (Gerhard Pirngruber)

20 **1. Introduction**

21 Vacuum gas oils represent a valuable source for high-quality refining products. An increase in
22 VGO hydroprocessing is connected with the changes in the composition of currently extracted
23 crude oils and market demand for lighter distillates. VGO consists of a large number of molecules,
24 including heterocyclic ones. Among these heteroatom-containing species, N-compounds are
25 highly problematic. These molecules are poisons for hydrotreating and hydrocracking catalysts,
26 and they exert an inhibitory effect on the removal of other heterocyclic compounds present in
27 VGOs [1–4]. At the same time, nitrogen-containing compounds also inhibit the catalytic cracking
28 conversion of VGO [5,6]. These species must be removed from the VGOs by catalytic
29 hydrotreatment before being subjected to further conversion processes.

30 In this work, we focus on the HDN reactions, i.e., on the elimination of N-containing species, as
31 these molecules are supposed to be the most refractory for hydrotreatment. In order to explain the
32 refractory behavior of the nitrogen-containing species and the kinetics of VGO HDT,
33 hydrotreatment studies of model molecules as pyridine [7–9], quinoline [10–13], acridine [14],
34 indol [15–17], and carbazole [14] were provided. These studies show the difference in the
35 reactivity and reaction pathways depending on the basic or neutral type of the molecule, the
36 position of the nitrogen atom, and the number of the aromatic rings. Typically, VGO contains
37 derivatives of these model molecules, whose structures are more complex due to additional
38 aromatic or naphthenic rings and/or alkyl side chains [18]. It is important to note that these
39 substituents can significantly influence the molecule's reactivity [19]. In addition, there are several
40 studies dedicated to the identification of HDN refractory species in real feeds as gas oils, vacuum
41 gas oils, and hydrotreated VGO effluents [20–26]. This knowledge is essential for kinetic
42 modelling of the HDT process.

43 As mentioned earlier, real feeds are affected by the structure of N-compounds and the presence
44 of other molecules. The diversity of structures of N-containing compounds in VGOs is determined
45 by the geochemical origin of crude oil and the process used to obtain VGO [27]. Typical processes
46 for producing VGOs are vacuum distillation of atmospheric residues (straight-run VGO),
47 hydroconversion, fluid catalytic cracking, visbreaking, or coking of heavy residues [28–30].
48 However, there is still a need to discuss the detailed characterization and a comparison of the
49 transformations occurring in VGOs of different process origins with various conversion degrees
50 in an HDT process. This data is a necessary step in the development of feed-independent kinetic
51 models of VGO hydrotreatment. In this work, we show a unique dataset of VGOs of different
52 origins. Based on it, we have compared the distributions of nitrogen-containing species in HDT
53 effluents from different types of feeds at a wide range of HDN conversion degrees.

54 FTICR-MS is a high-resolution analytical technique that provides molecular formulas of species
55 containing heteroatoms in a complex hydrocarbon mixture [31]. The application of an electrospray
56 ionization source allows selective analyzing of two types of nitrogen-containing species. The
57 separation of basic and neutral species is important as the molecules within one type have similar
58 reaction pathways, which is essential for reaction network construction [32]. VGOs and HDT
59 effluents have their own “fingerprints,” frequently presented in the form of derivatives of Kendrick
60 plots showing the alkylation and aromaticity degrees of the molecules present in the mixture
61 [33,34]. The alkylation degree is determined by the number of carbon atoms (n_C). The aromaticity
62 is described by a double bond equivalent (DBE), expressed by Eq.1 for a $C_cH_hN_nO_oS_s$ molecule:

63
$$DBE = c - \frac{h}{2} + \frac{n}{2} + 1 \quad (1)$$

64 DBE is a method of calculating the aromaticity or unsaturation degree when the molecular
65 formula is known. It indicates a number of double or triple bonds and rings in the molecule. For

66 example, DBE=3 may correspond to a structure with 3 rings or 2 rings and one double bond. At
67 the same time, this method gives wrong values for complex organic molecules containing multiple
68 elements, which may have different valence states. The compounds containing halogens have
69 negative DBE values. We use the DBE method as it is a fast and accurate method of determining
70 the aromaticity of the species studied in this work, but we cannot use it to completely distinguish
71 between aromatic structures and hydrogenated structures with additional rings.

72 The previous studies reported that VGOs contain different heteroatom groups (i.e., NI , $NxSy$,
73 SI , $OxNy$), but the NI class (only one nitrogen atom in the structure) is predominant. In addition,
74 multi-heteroatom species are very quickly removed during hydrotreatment or reduced to a very
75 small residual concentration [33]. In this work, we focus on the comparison of the species and their
76 families containing only one nitrogen atom in a structure.

77 This paper begins with a description of the pilot tests and experimental conditions used for
78 obtaining HDT effluents, physicochemical characteristics of the studied VGOs and corresponding
79 effluents. We present the conditions applied for the (ESI+/-)-FTICR-MS analysis. The next section
80 contains the results of the comparison of the effluents at different HDN conversion degrees by
81 DBE and the number of carbon atoms. In the discussion section, we propose mechanisms for VGO
82 HDN based on the obtained data and compare our results with the relevant studies of heavier and
83 lighter cuts. Our conclusions and perspectives of the study are drawn in the final section.

84

85 **2. Experiments and methods**

86 *2.1. Feedstocks*

87 The feedstocks are four industrial vacuum gas oils of different types: two straight-run vacuum
88 gas oils (SR VGO) obtained from direct distillation of crude oils, one heavy coker gas oil (HCGO)

89 produced via a thermal conversion process, and one hydroconverted vacuum gas oil (HVGO)
90 obtained via hydroprocessing of heavy residues.

91 2.2. Pilot tests

92 The VGO hydrotreatment tests were performed in a pilot unit equipped with an up-flow fixed-
93 bed catalytic reactor over a $NiMo/Al_2O_3$ commercial catalyst. The experimental unit can be divided
94 into three major sections: the feed, the reaction, and the separation section (Fig. A.1). The feed
95 section consists of the hydrogen line (purity=99.5 %) and the hydrocarbon liquid feed section. The
96 hydrocarbon feed section is composed of two feed tanks (in Fig. A.1, only one tank is illustrated)
97 and two transfer pumps. To keep the feed in a liquid phase, these pieces of equipment are inside
98 the heated enclosure. The hydrocarbon feed and H_2 are injected together from the bottom of the
99 reactor via a mixing gas-liquid inlet. The reactor itself is a steel tube with a volume of 165 cm^3
100 and with an internal diameter of 19 mm. The catalytic bed is packed with glass balls (0.5 mm
101 diameter) and carborundum layers. A 1 cm grid is placed at the end of the catalytic bed in order to
102 hold the catalyst in place. The catalyst's volume is 50 cm^3 with an additional 10 cm^3 of catalyst
103 guard bed, protecting the main catalyst from deactivation by metals.

104 Four heating shells around the reactor provide an isothermal axial temperature profile in the
105 catalyst zone. Each heating shell contains an external thermocouple. The internal thermal profile
106 is controlled and regulated by four internal thermocouples (TC). These four TCs are spread over
107 the height of the reactor in order to have an internal measurement per heating shell.

108 Before entering the separation section, the reactor effluent is kept at a high temperature to
109 prevent plugging caused by the creation of ammonium sulphide crystals. The high-pressure
110 separator V1 separates the effluent into a liquid phase, which will be sent to the collecting tank,

111 and a gas phase, which will be directed to the separator V2. Separated gases from V2 are sent
112 automatically to gas chromatography every 4 hours.

113 Operating conditions were chosen by preliminary simulation of HDT and HDN performance to
114 cover the full range of conversion of nitrogen-containing species in the pilot tests. All pilot tests
115 were started from a reference point with the same VGO feed to check the repeatability of the
116 experiments. The reference point was repeated to evaluate the catalyst deactivation at the end of
117 each test. To control the stabilization of the experimental points, we monitored the macroscopic
118 properties (density, refractive index, sulphur, and total nitrogen content) of the liquid phase and
119 the composition of gas effluents. Once we achieved stable operation, a mass balance was
120 performed, taking into account analyses of the feed (gas + VGO) and the product (online gas
121 analysis + hydrotreated effluent).

122 Pilot tests were carried out under the conditions described in Table 1 for a period of 38-45 days.
123 The conversion of the nitrogen in the effluent after hydrotreatment was calculated via the following
124 equation (Eq.2), where $c[N]_i$ - the content of the total nitrogen in the VGO (in ppm) and $c[N]_o$ -
125 the content of the total nitrogen in the hydrotreated effluent (in ppm):

126

127 **Table 1**

128 Pilot tests operating conditions.

H_2 partial pressure, bars	120
Temperature, °C	$T_{ref}-20 - T_{ref}+35$
LHSV, h ⁻¹	$LHSV_{ref}-0.9 - LHSV_{ref}+2.1$
H_2/HC ratio, NL/L	900

129

130
$$HDN = \frac{c[N]_i - c[N]_o}{c[N]_i} \cdot 100 \% (2)$$

131

132 2.3. (ESI+/-)-FTICR-MS

133 VGOs and effluents were analyzed by FTICR-MS in ESI(+) and ESI(-) modes to characterize
134 basic and neutral nitrogen compounds, respectively. In order to assess the reproducibility of the
135 tests, three replicate analyses were carried out on each sample. Mass spectrometry was done using
136 an LTQ FT Ultra Mass Spectrometer FTICR-MS (ThermoFisher Scientific) equipped with a 7T
137 magnet (Oxford Instruments), with an ESI source (ThermoFisher Scientific, Bremen, Germany).
138 The data acquisition range was set to m/z of 98-1000, with 200,000 initial resolution, and 70 scans
139 were collected for each sample. The transient signal was recorded to enable further data processing.
140 The ionization parameters were used based on the results of Guillemant's FTICR-MS study of
141 nitrogen compounds in gas oils [35].

142 The samples with a total nitrogen content above 100 ppm were prepared using a VGO
143 concentration of 0.5 mg/mL in a toluene-methanol solvent in a proportion of 75:25 % v/v with 1%
144 of additive (acetic acid or ammonium hydroxide depending on the ionization mode). For samples
145 with a total nitrogen content of less than 100 ppm, the (ESI+)-FTICR-MS data was too noisy under
146 these conditions. In order to avoid this problem, these samples were prepared using a higher VGO
147 concentration of 1 mg/mL. Fig. A.2 presents the comparison of the basic family distributions by
148 relative intensities for effluent B3 (Table A.1), originating from SR VGO B, and obtained at 88 %
149 of HDN, containing 339 ppm of nitrogen. This nitrogen content allows obtaining (ESI+)-FTICR
150 mass spectra for the samples prepared with low and higher concentrations of VGO. The results
151 show good reproducibility of the peak intensities at elevated concentrations, enabling comparison
152 of all hydrotreated effluents samples.

153 PeakByPeak and Autophaser commercial software provided transient summation, phase
154 correction, threshold noise extraction, peak selection, and mass recalibration. More details on the
155 used processing procedure can be found in the work of Guillemant et al. [36].

156 Obtaining a quantitative composition by (ESI)-FTICR-MS remains an unachievable task due to
157 the non-uniform ionization of the molecules. For the semi-quantitative characterization of the N-
158 containing species, we used the approach described in the Nguyen et al. study [20]. Pseudo-
159 concentrations are presented as the product of the relative intensities in ESI(+) or ESI(-)-FTICR-
160 MS spectra and the basic/neutral nitrogen content of the VGO or its HDT effluents.

161 As previously stated, in this study, we focused on the families of the *NI*-class. To characterize
162 the species of this class, we linked the corresponding DBEs to each family, named after the
163 simplest structure (without side alkyl chains and extra aromatic or naphthenic rings) representing
164 the family. Fig. 1 describes the representative structures and DBE intervals for the studied *NI*
165 families.

166

167 **3. Characterization of feedstocks and effluents**

168 In this work, feeds and liquid effluents were analyzed by standard petroleum analyses and
169 (ESI+/-)-FTICR-MS. Table A.2 describes the standards or the methods of the used analyses.

170 The physicochemical properties obtained from standard petroleum analyses of the feeds and
171 corresponding liquid effluents are given in Table 2 and Table A.1. More details on the simulated
172 distillation curves of the studied vacuum gas oils can be found in Fig. A.3. Besides the process
173 origin, the selected feeds differ by the content of total nitrogen, basic nitrogen, sulfur, and density.
174 Feeds C and D, which originate from conversion processes of heavier fractions, have higher
175 nitrogen contents than the SR VGOs A and B. Feed D has a particularly low sulfur content since

176 it is a product of hydrotreating. The initial and final boiling points of the feeds vary from 227 to
177 291 °C and 588 to 603 °C, respectively. Feed C is the lightest one of the four VGOs.

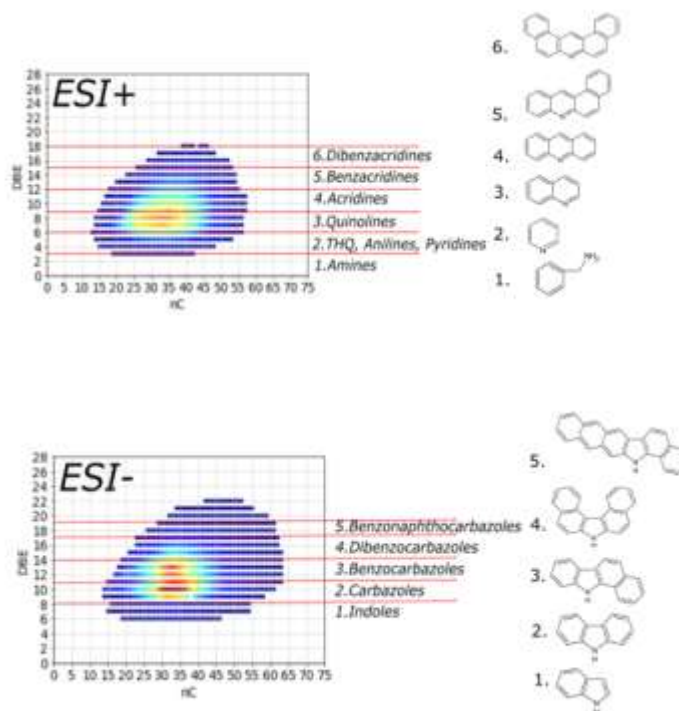
178 More details on the differences between the feeds can be observed by comparing the DBE vs.
179 the number of carbon atom plots in Fig. 2. Additional information can be extracted from these
180 plots using a planar limits approach, which allows evaluating the difference in the types of the
181 present structures in vacuum gas oils [26,37]. In the DBE-nC plots, we estimate the slope of the
182 line that connects the points with the highest DBE at the range of numbers of carbon atoms in the
183 N-containing species. In Fig. A.4, three variants of planar limits slopes are demonstrated by the
184 example of the basic nitrogen-containing molecules. The slope of 0.75 implies an increase in DBE
185 by 0.75 per carbon atom, which corresponds to the linear addition of an aromatic ring. If a slope
186 is above 0.75 (DBE is increased by more than 0.75 per carbon atom), it indicates a non-linear
187 aromatic ring addition. The slope below 0.75 is characteristic of a saturated ring or an alkyl chain
188 addition. The same interpretation of the slopes is also applicable to the neutral type of nitrogen-
189 containing species.

190 *3.1.Characterization of straight-run VGO A*

191 SR VGO A has the lowest total nitrogen content and the lowest density (Table 2) among the four
192 feeds. The boiling range of this feed is 285-602 °C, and the nitrogen to sulphur ratio (N/S) is 0.09.

193 For the SR VGO A (left column in Fig. 2), the basic *NI* molecules are characterized by a DBE
194 range of 4-22 and carbon numbers 11-61 with highly intensive peaks (relative intensity above 40
195 %) at DBE 7-13 and carbon numbers 25-44. The carbon number distribution for basic nitrogen
196 species in VGO A is centered between 30 and 35 carbon atoms, with the maximum at DBE=9
197 (quinoline with two saturated rings structures). In the case of SR VGO A, the planar limit slope is
198 close to 0.75. It means that for basic N-species of SR VGO A with an increase in DBE from 8 to

199 18, the structures of the species represent the product of the linear addition of aromatic rings to
200 structures with a lower DBE.



201
202 **Fig. 1.** NI-families representative structures and corresponding DBE ranges for ESI+ and ESI-
203 modes.

204 When comparing the DBE vs. a number of carbon atom plots for neutral NI species (right
205 column in Fig. 2) in VGO A, one can see that the distribution is characterized by the range of
206 DBE=6-22 and the range of carbon atoms nC=15-57. The most abundant peaks are found at
207 DBE=12 and DBE=13 (benzocarbazoles) in the range of nC from 30 to 35. VGO's A DBE-nC
208 plot obtained in negative ESI mode shows a slope characteristic for linear aromatic addition.

209 3.2.Characterization of straight-run VGO B

210 SR VGO B has a medium total nitrogen content and the highest density (Table 2) among the
211 four feeds. The boiling range of this feed and N/S ratio are very close to SR VGO A and equal to
212 291-603 °C and 0.08, respectively.

213 For the SR VGO B, the basic *NI* molecules distribution is characterized by a DBE range of 4-
214 19 and carbon numbers 11-58 (Fig. 2). The most intensive peaks (relative intensity above 40 %)
215 are located at DBE=7-13 and carbon numbers 25-44, similarly to SR VGO A. The carbon number
216 distribution for basic nitrogen species in VGO B is centered between 30 and 35 carbon atoms, with
217 the maximums at DBE=8 and DBE=9 (quinoline structures with one and two saturated rings,
218 respectively). The planar limit slope is 0.76, i.e., the same as in SR VGO A.

219 The differences at the molecular level between two straight-run VGOs are more evident when
220 comparing the DBE vs. a number of carbon atom plots for neutral N-species. SR VGO B has a
221 narrower DBE-nC distribution (DBE=9-20, nC=16-50) compared to VGO A. The common feature
222 in the two SR VGOs is the location of the most abundant peaks at DBE=12 and 13 and the most
223 intensive species have from 30 to 35 carbon atoms. In contrast to the basic nitrogen distributions,
224 the two SR VGOs have different slopes of planar limits of the neutral N-species (Fig. 2). The slope
225 of VGO B is lower than 0.75, indicating the addition of saturated carbon atoms with an increase
226 in DBE.

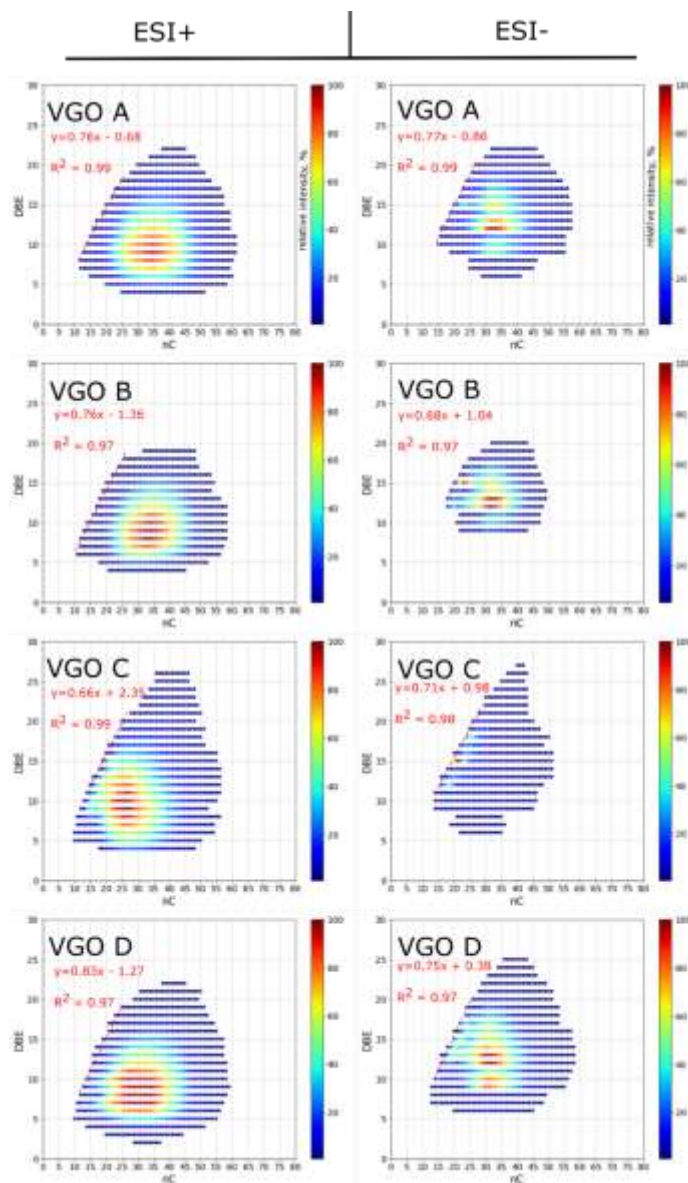
227 *3.1.Characterization of heavy coker gas oil VGO C*

228 HCGO VGO C has a high total nitrogen content and a medium density (Table 2). The initial
229 boiling point of this feed is low (227 °C), and the final boiling point is lower than in the SR VGOs
230 (588 °C). VGO C's N/S ratio is twice higher than in SR VGOs.

231 The basic *NI* species in VGO C are located in the zone DBE 4-27 and carbon numbers 10-56.
232 In comparison to SR VGOs, the most abundant peaks in HCGO are in the similar zone of DBE 7-
233 13, but these species have shorter alkyl side chains (nC 21-33). The most abundant species in
234 HCGO are quinolines with two saturated rings (DBE=9) and acridines (DBE=10). For VGO C, a
235 slope below 0.75 was observed, which can probably be explained by the presence of saturated

236 rings addition. One can see that for HCGO VGO C, the most abundant peaks are close to the planar
237 limit, which is related to the short alkyl chains of nitrogen compounds in this type of feed.

238 The most abundant neutral nitrogen species in HCGO are presented only by a few separate points
239 with an alkylation degree of less than 26 carbon atoms at DBE=12, 15, and 18. For neutral N-
240 species, the slope of the planar limit was also below 0.75.



241
242 **Fig. 2.** DBE vs. carbon atom number plots for basic (ESI+ column) and neutral (ESI- column)
243 *N*I compounds in the feeds (VGO A, VGO B - SR VGO, VGO C - HCGO, VGO D - HVGO).

244 **Table 2**

245 Physicochemical properties of the feeds.

Sample	d ₁₅ , g/cm ³	N total, wppm	N basic, wppm	N neutral, wppm	S, wppm	IBP, °C	FBP, °C
VGO A (SR VGO)	0.9212	1440	396	1044	15620	285	602
VGO B (SR VGO)	0.9787	2650	697	1953	34600	291	603
VGO C (HCGO)	0.9495	3425	892	2533	16720	227	588
VGO D (HVGO)	0.9317	3640	1059	2581	3409	264	589

246

247 *3.2.Characterization of hydroconverted vacuum gas oil VGO D*

248 HVGO VGO D has the highest total nitrogen content and medium density (Table 2). The initial
 249 boiling point of this feed is 264 °C and the final boiling point is the same as that of VGO C, 589
 250 °C. VGO D has the highest N/S ratio of the four feeds.

251 Regarding *NI* basic species in HVGO (VGO D), one can see that its fingerprint is located in the
 252 DBE zone with values 2-22 and nC values 10-59. The most intensive peaks are slightly less
 253 aromatic (DBE range 6-11), and their alkylation degree is wider compared to the three other feeds.
 254 The most abundant basic nitrogen species in HVGO have 25-35 carbon atoms. The slope of the
 255 planar limit is 0.83, which indicates the presence of peri-condensed aromatic rings.

256 The distribution of neutral N-species in VGO D looks similar to SR VGO A. However, the most
 257 abundant species are more intensive at DBE=9-10 and 12-13, which are centered at 30-35 carbon
 258 atoms. The planar limit slope of VGO D is also close to the value of the slope in VGO A, which
 259 shows a linear addition of aromatic cycles.

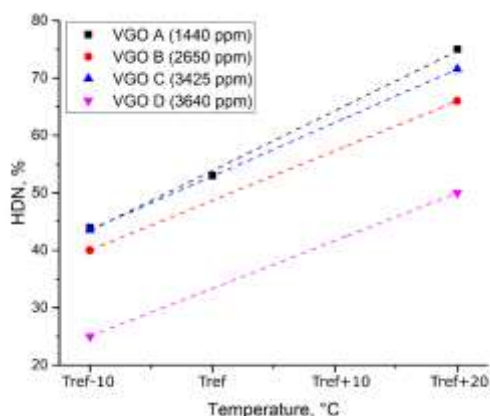
260 The essential advantage of the selected feeds is the difference in the DBE-nC distributions of
 261 the abundant neutral and basic species, which makes it possible to work with a wide variety of
 262 structures. It is important to note that the distributions of the most intensive peaks share common

263 trends for VGOs of the same type (i.e., SR). For better understanding, the simplest hypothetical
264 structures of the most abundant species in each feed are illustrated in Fig. A.5.

265

266 4. Results

267 In order to evaluate the reactivity of the feeds, the HDN conversion as a function of temperature
268 was compared for each feed. Fig. 3 shows the dependence of HDN on the temperature in the reactor
269 at a constant liquid hour space velocity (LHSV). According to the plot, SR VGO A demonstrated
270 the highest reactivity, closely followed by HCGO (VGO C) and SR VGO B. HVGO (VGO D)
271 showed the lowest reactivity during the pilot tests.

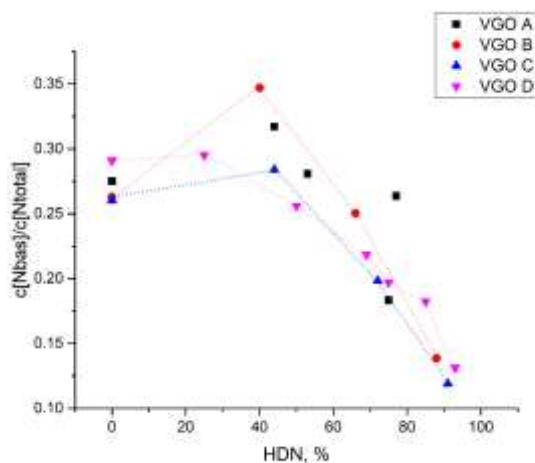


272

273 **Fig. 3.** Comparison of the feeds reactivity (experimental HDN vs. temperature in the reactor) at
274 fixed LHSV.

275 To better understand the differences between the selected feeds during HDT, we have provided
276 a comparison of the distributions of neutral and basic families as a function of HDN conversion.
277 It is worth noting here that during hydrodenitrogenation of all feeds we observed a slight increase
278 in the basic nitrogen compounds' fraction at the beginning of the hydrotreatment (Fig. 4). It can
279 be explained by the fast consumption of the neutral nitrogen species or by the transformation of

280 neutral nitrogen species into basic ones. At high HDN conversions, however, the basic nitrogen
 281 species were almost completely converted, and the majority of the “refractory” (or residual)
 282 nitrogen species were neutral ones, which is explained by reactivity differences due to competitive
 283 adsorption on the catalyst’s surface [14,17,38]. While all feeds follow the same global trend, the
 284 operating conditions also impact the basic fraction. This is visible for VGO A, where we observed
 285 two very different values for the basic nitrogen fraction at close to 75 % HDN conversion. This is
 286 attributed to different reaction temperatures: at a given conversion, a lower temperature led to a
 287 higher fraction of basic nitrogen in the effluent. More peculiarities of these effects in vacuum gas
 288 oils can be provided after a detailed analysis of the nitrogen families’ transformations as a function
 289 of HDN degree.



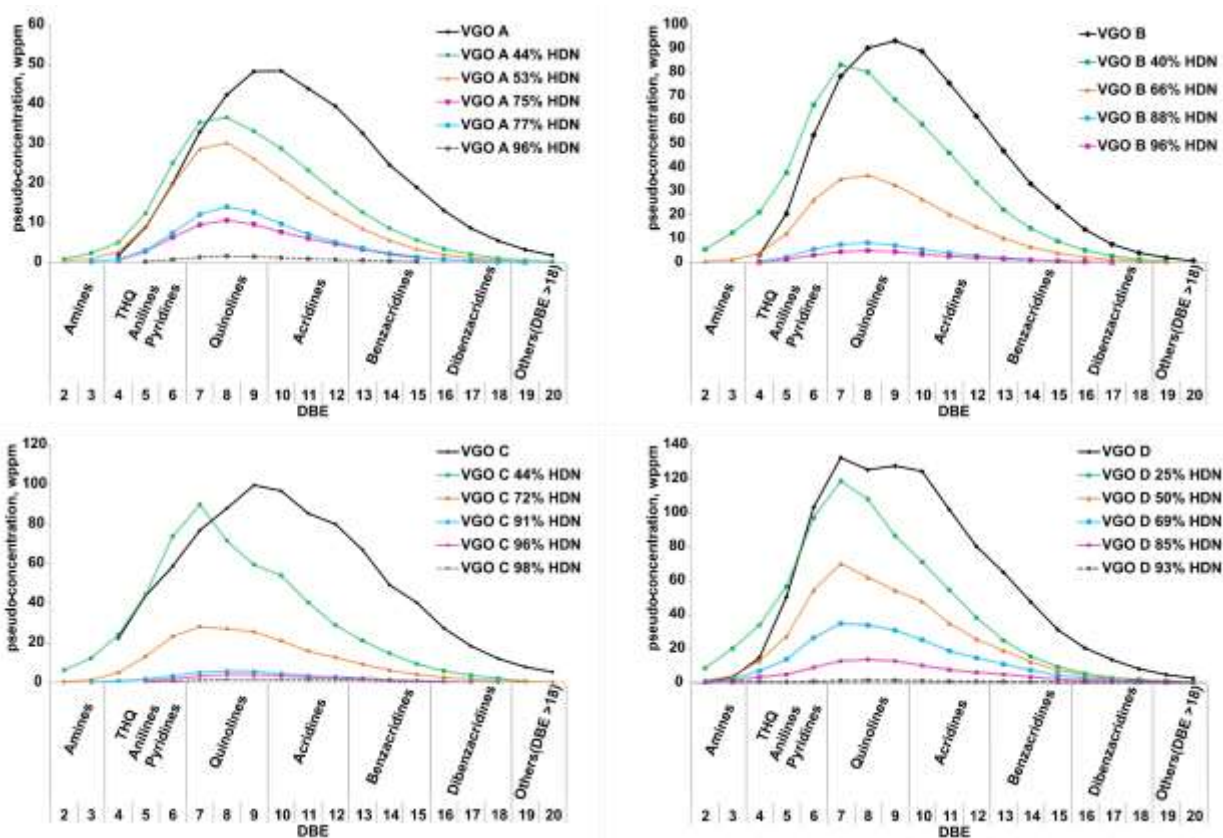
290
 291 **Fig. 4.** Change in the proportion of basic nitrogen as a function of HDN level.

292 *4.1. Transformation of basic and neutral nitrogen species*

293 *4.1.1. Changes in DBE distributions for SR VGO A*

294 A comparison of the distributions of the basic nitrogen families as a function of DBE is shown
 295 in Fig. 5. A normal distribution was observed for SR VGO A and its effluents at all conversion
 296 degrees. The distribution maximum shifted from DBE=9 to DBE=7 at the start of hydrotreatment,

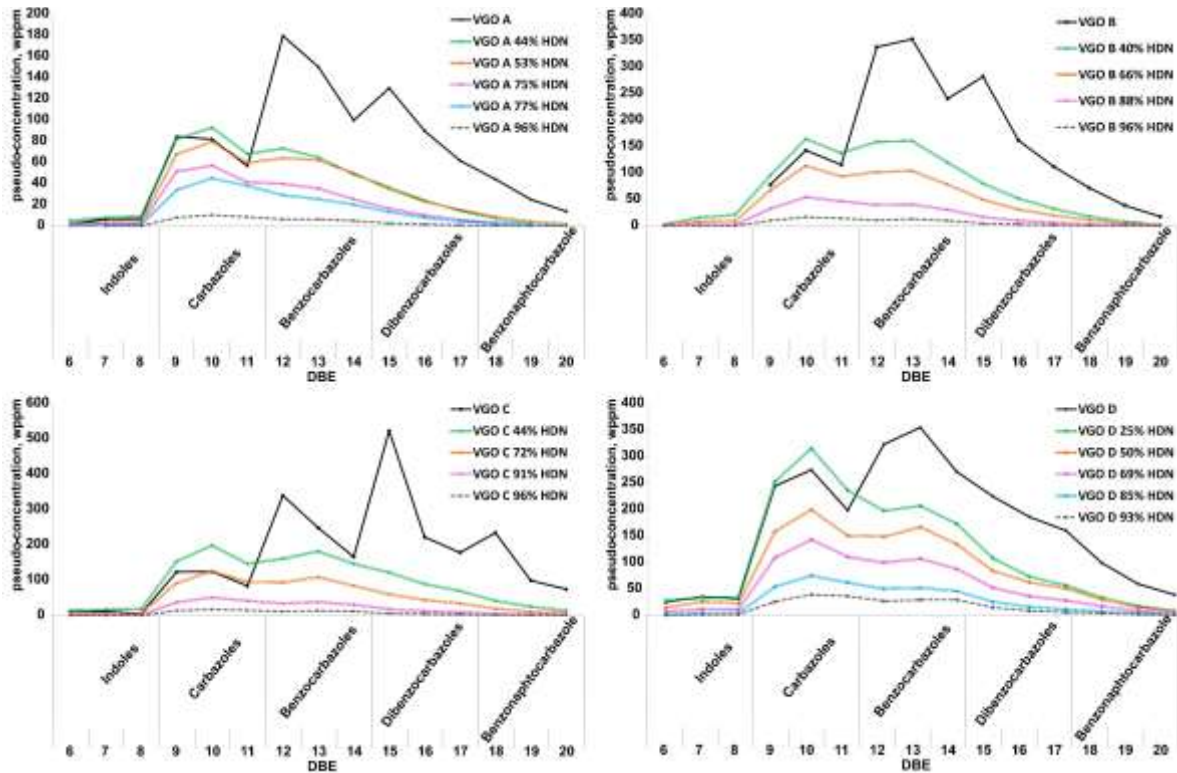
297 and the pseudo-concentration of the families with DBE=7-20 decreased. The DBE shift of -2
 298 happened due to the hydrogenation of one aromatic ring in the highly aromatic structures. After
 299 53 % of HDN, the structures with DBE=8 were the most abundant in the effluents. The distribution
 300 of families in the hydrotreated effluents ranged from amines (DBE=2) to dibenzacridine families
 301 (DBE=18). The full transformation of the most aromatic basic species (DBE=16 and higher) was
 302 observed only at 96 % of HDN.



303
 304 **Fig. 5.** The distributions of the basic nitrogen families at different HDN conversion degrees.

305 Fig. 6 reports a detailed comparison of neutral nitrogen families. As one can see, SR VGO A
 306 has a trimodal distribution for the initial feed (the carbazole, benzo- and dibenzocarbazole families
 307 had the most intensive peaks) with a high proportion of benzocarbazoles with DBE=12.

308 The trends for the neutral nitrogen species show rapid consumption of the neutral species with
 309 high DBEs as benzocarbazoles, dibenzocarbazoles, and benzonaphthocarbazoles at early
 310 hydrotreatment stages. After 44 % of HDN, a slow uniform consumption of the carbazoles and
 311 benzocarbazoles was observed. Even at high conversion degrees, some amounts of the species at
 312 DBE range from 9 to 15 remained in the effluents.



313
 314 **Fig. 6.** The distributions of the neutral nitrogen families at different HDN conversion degrees.

315 *4.1.2. Changes in DBE distributions for SR VGO B*

316 The second SR VGO B and its effluents also demonstrate a normal DBE distribution for basic
 317 N-species (Fig. 5), spanning from amines to dibenzacridines at conversion degrees up to 88 % of
 318 HDN. As for SR VGO A, we observed a shift of the distribution maximum from DBE=9 to DBE=7
 319 in the early process. Species with DBE=7 predominated at a low conversion rate (HDN=40%) in
 320 VGO B. At higher HDN conversion, the maximum shifted to DBE=8.

321 Concerning neutral N-species in SR VGO B, similar to SR VGO A, a trimodal distribution was
322 observed for the initial feed, with a predominance of benzocarbazoles with DBE=12 and DBE=13
323 (Fig. 6). Analogous to the first SR VGO, the neutral species with DBE above 12 were rapidly
324 consumed at the beginning of hydrotreatment. After 44 % of HDN, there was a slow uniform
325 consumption of the carbazoles and benzocarbazoles.

326 *4.1.3. Changes in DBE distributions for HCGO VGO C*

327 In the case of basic nitrogen-containing species in HCGO VGO C, the distribution's maximum
328 shifted from DBE=9 to DBE=7 at the beginning of the hydrotreatment and after then returned to
329 DBE=9 with increasing HDN (Fig. 5). This behavior could be attributed to the fast hydrogenation
330 of species with DBE=9, leading to the increase of species with DBE=7 at the beginning of HDT
331 and to the sluggish hydrogenation of DBE=10-13 species whose pseudo-concentration is quite
332 high in the HCGO, leading to the shift back to DBE=9 at higher conversion.

333 HCGO has a DBE distribution for neutral species with four peaks at carbazole, benzo- and
334 dibenzocarbazole and benzonaphthocarbazole families. In the first HDT effluent (44 % of HDN),
335 one can see a very quick consumption of a part of benzocarbazoles, dibenzocarbazoles, and species
336 with DBE=18 (Fig. 6).

337 *4.1.4. Changes in DBE distributions for HVGO VGO D*

338 We observed a different DBE distribution pattern for the basic N-species in the hydroconverted
339 VGO D compared to the previous three feeds. The first thing that is striking is the wider DBE
340 distribution, which is typical for HVGO, which is the product of hydrotreatment of heavier feeds
341 (Fig. 5). Likewise, the shift from DBE 9 to 7(8) was not observed, presumably because the feed
342 had already been hydrotreated, which means that the shift had already occurred in the feed.

343 The effect of preliminary feed hydrotreatment is also visible in the neutral species, where the
344 fraction of species with DBE=10 and DBE=12 is significantly higher than in other feeds (Fig. 6).

345 *4.2. Changes in alkylation degree*

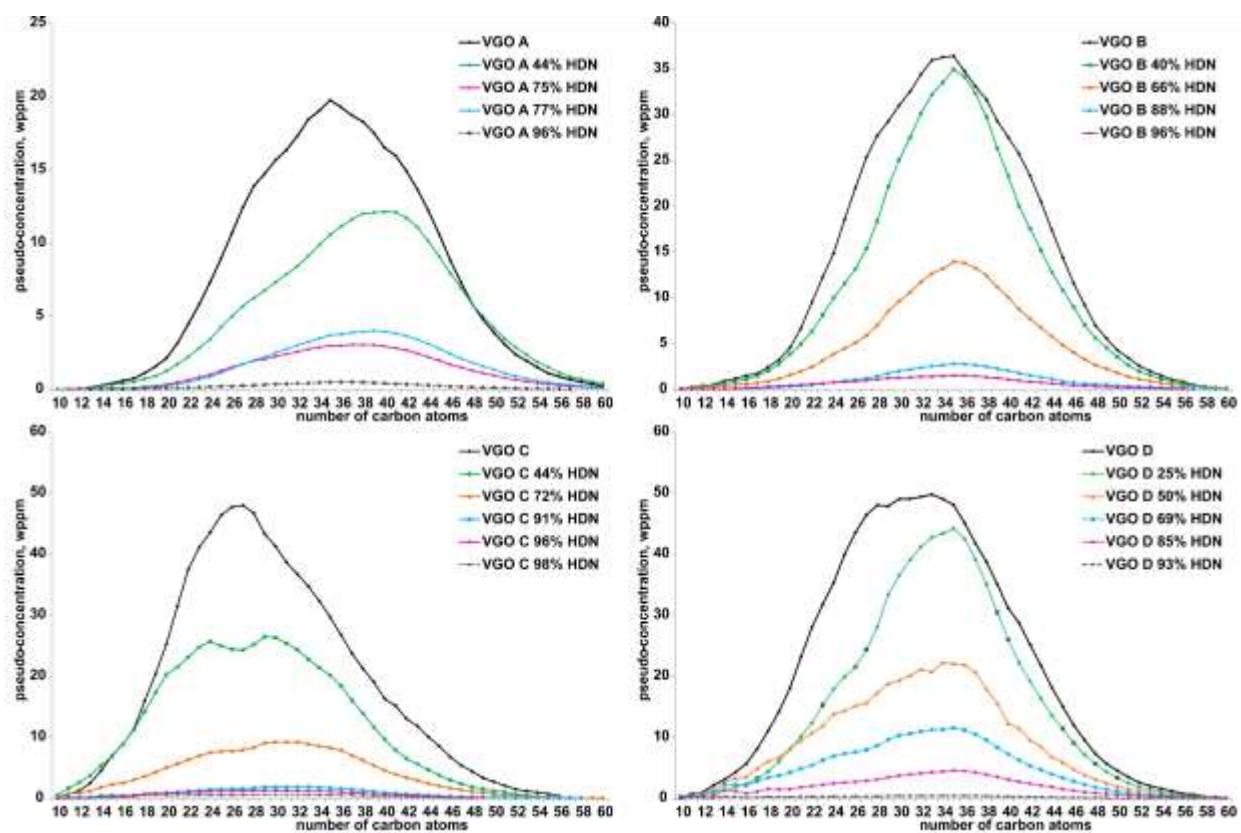
346 In order to verify the origin of basic nitrogen species (hydrogenation of the basic species with
347 higher DBE vs. hydrogenation of the neutral species) and to understand the HDN reaction
348 mechanism of the species, it will be informative to study the carbon number distributions for the
349 most abundant DBEs for basic and neutral species and for those with higher DBEs that are likely
350 to be the source of abundant species in the HDT effluents. Fig. 7-8 show the carbon number
351 distributions for all N-families and conversion degrees for positive and negative electrospray
352 ionization modes, respectively. Substantial information about species' reactivity can be extracted
353 by a detailed analysis of these distributions for all N-families.

354 *4.2.1. Changes in carbon number distributions for SR VGO A*

355 For VGO A, the less alkylated basic nitrogen species were rapidly consumed at the beginning
356 of hydrotreatment (Fig. 7), leading to a shift of the distribution's maximum to the right. The least
357 reactive basic species had a carbon number above 47. For the neutral species, all carbon numbers
358 diminished to roughly the same extent at the early stages; the distribution shifted to heavier species
359 only at higher conversion levels (Fig. 8).

360 To extract more information about the origin of the most abundant species in the effluents, the
361 carbon number distributions for basic species in VGO A with DBE=7, DBE=8, DBE=9, DBE=11
362 were compared (Fig. A.6). From the study of DBE distributions described in the previous section,
363 it was found that there was a shift towards quinolines and species with DBE=7 at the beginning of
364 hydrotreatment. Comparing the carbon number distributions for these species, one can see
365 consumption of the quinolines with DBE=7 and carbon atoms from 24 to 36, while heavier ones

366 were slightly accumulated. The accumulation of DBE=7 species compared to initial feed can be
 367 related to the hydrogenation of quinolines with DBE=9, resulting in structures with one aromatic
 368 cycle. At the same time, quinolines and species with DBE=9 can originate from acridines with one
 369 saturated cycle characterized by DBE=11. Quinolines with DBE=9 and carbon atoms in the range
 370 14-45 were rapidly consumed, whereas the pseudo-concentration of species with a number of
 371 carbon atoms above 45 remained at the same level as in the initial feed. The accumulated DBE=7
 372 species with higher carbon atom numbers (in the case of VGO A, above 45) were probably
 373 generated from neutral nitrogen species.

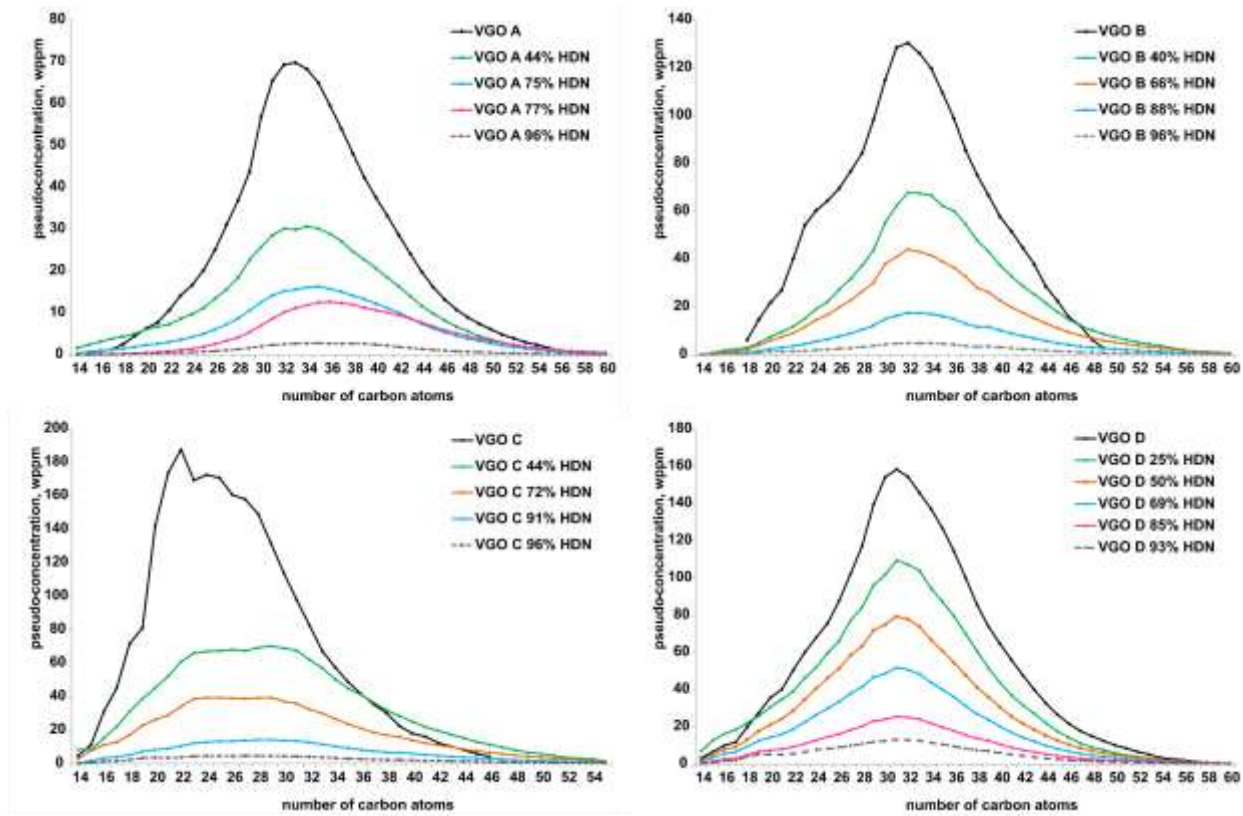


374
 375 **Fig. 7.** The carbon number distributions of the basic nitrogen families at different HDN conversion
 376 degrees.

377 The shift of the carbon distributions' maximum from 35 to higher carbon numbers at the
378 beginning of the hydrotreatment indicates a higher reactivity of species with low carbon number
379 in the feed.

380 In Fig. A.7, the carbon number distributions are shown for the most abundant neutral nitrogen-
381 containing families in DBE distributions: carbazoles with DBE=10, benzocarbazoles with
382 DBE=12 and their potential sources - families with DBE=14 and DBE=16. Carbazoles with
383 DBE=10 may originate from benzocarbazoles with DBE=12 by hydrogenation of an external
384 aromatic cycle. At the early stages of HDN, the consumption of carbazoles and their generation
385 by hydrogenation of benzocarbazoles are in balance.

386



387
388 **Fig. 8.** The carbon number distributions of the neutral nitrogen families at different HDN
389 conversion degrees.

390 4.2.2. *Changes in carbon number distributions for SR VGO B*

391 For VGO B, basic nitrogen species hardly diminished at low HDN level, probably due to a
392 transfer from the neutral to the basic fraction; in contrast to VGO A, there was no change in the
393 distribution of carbon numbers (Fig. 7). As for the neutral species, they diminished more quickly
394 at low conversion, without any marked change in the carbon number distribution (Fig. 8). In the
395 distribution of carbon numbers for neutral nitrogen species, one can see the generation of highly
396 alkylated species within the HDN level. We attribute this to the semi-quantitative nature of the
397 analytical technique or to the possible generation of these neutral N-species from the other
398 heteroatom-containing minor classes as *NIOx*, *NISx*, etc., during the hydrotreatment.

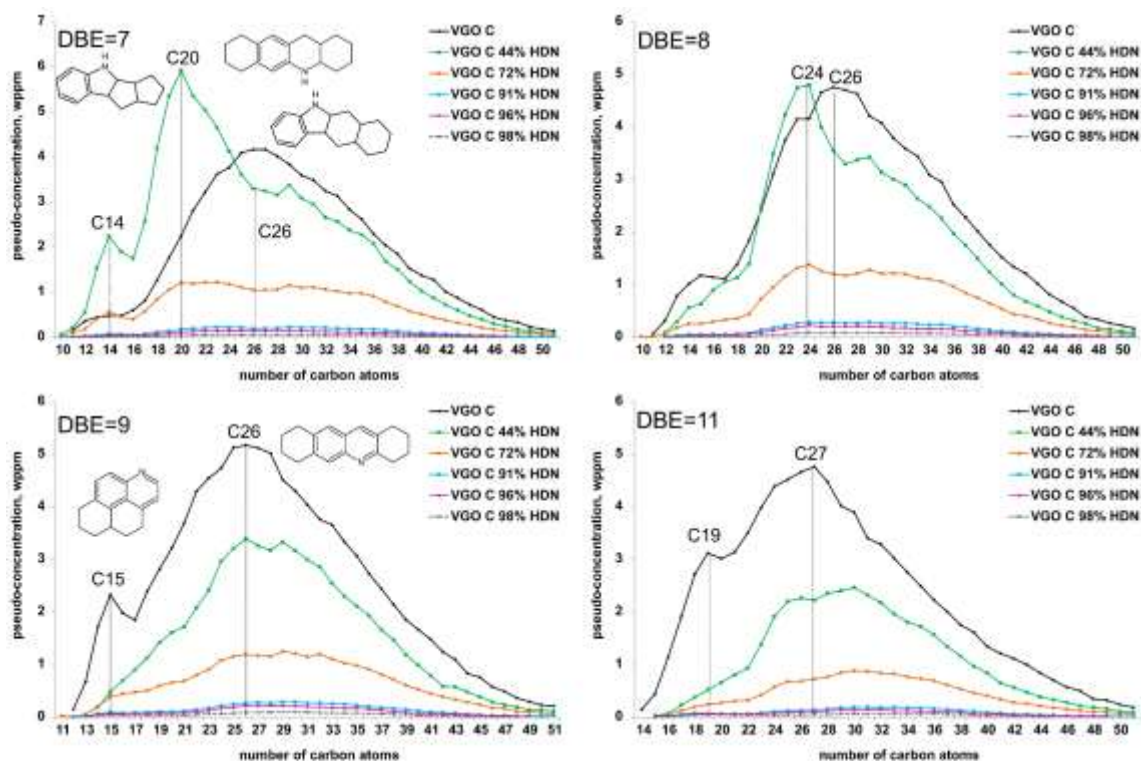
399 As in the previous VGO, the carbon number distributions for the most abundant basic and neutral
400 N-species in VGO B were compared (Fig. A.8-A.9), and trends qualitatively similar to those in
401 the case of SR VGO A were observed.

402 4.2.3. *Changes in carbon number distributions for HCGO VGO C*

403 We noted a faster consumption of highly alkylated basic species in the carbon number
404 distribution for VGO C (Fig. 7), i.e. the opposite trend than in feed A. As for the carbon number
405 distribution for neutral nitrogen species shown in Fig. 8, effluents were found to have a broader
406 distribution compared to the initial feed. The generation of highly alkylated neutral compounds
407 within HDN conversion is also assumed to be an artefact, attributed to the conversion of *NIOx*
408 and/or *NISx* species to the *NI* family.

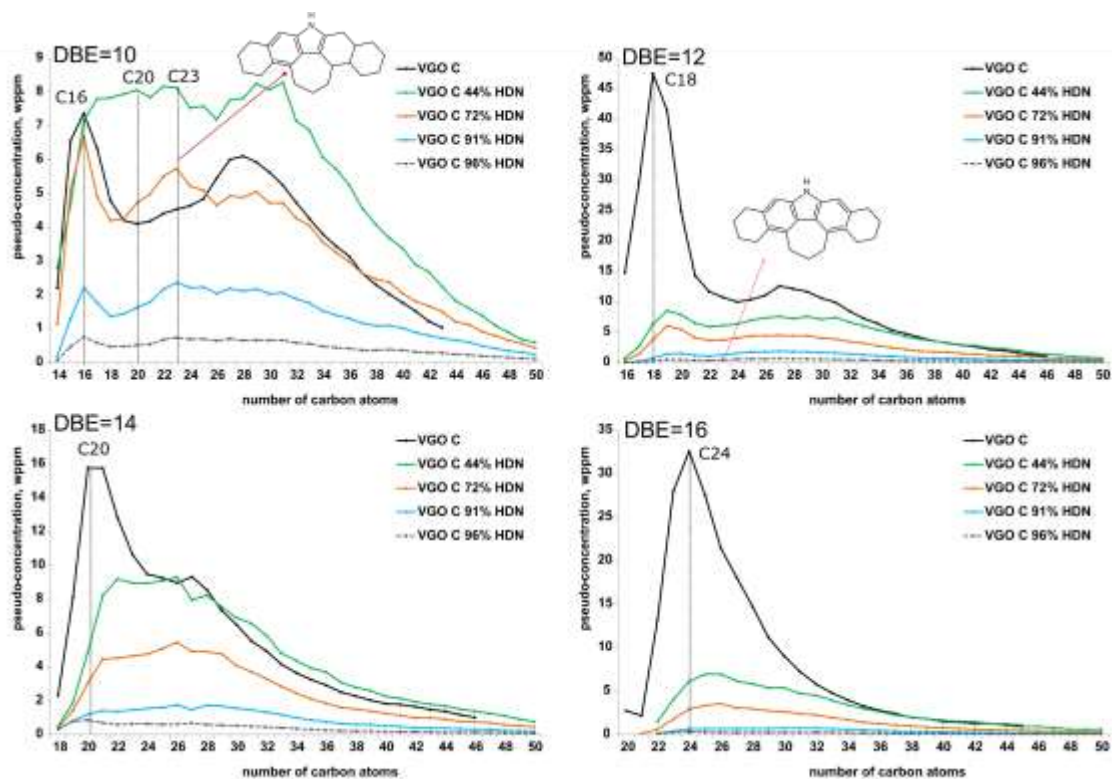
409 As can be seen from Fig. 9, for species with DBE=7, there was a strong accumulation of basic
410 species with 14 and 20 carbon atoms at the early HDT stages. Comparing these results with the nC
411 distribution for neutral species (Fig. 10), we observed a very fast consumption of a peak of
412 DBE=12 species (benzocarbazoles) with a low carbon number. We assume that full hydrogenation

413 of the aromatic cycle next to the heteroatom-containing ring occurred, leading to its transition into
 414 basic-type species with DBE=7. The light species with C14 probably also originated from neutral
 415 nitrogen species, containing five-membered cycles. Hypothetical structures with DBE=7 and 14
 416 carbon atoms are suggested in Fig. 9. Given that the basic species with DBE=9 and DBE=11 are
 417 consumed uniformly throughout the nC range, they also can contribute to the accumulation of the
 418 species with DBE=7, but do not explain the peak at 20 carbon atoms. For DBE=9 and DBE=11, a
 419 bimodal distribution was observed. We evoke the hypothesis that the bimodal distribution arises
 420 from the simultaneous presence of structures with different numbers of rings, i.e. in the case of
 421 DBE=9, three-rings (acridine), and four-rings (dinaphtoquinoline) and the presence of the peri-
 422 condensed structures. The hydrogenation of DBE=9 compounds responsible for the peak at low
 423 carbon numbers could explain the peak at C14 in the DBE=7 distribution at low HDN conversion.



424
 425 **Fig. 9.** The carbon number distributions of the quinolines (DBE=7-9) and acridines (DBE=11) in
 426 VGO C.

427 Returning to the carbon number distribution of neutral N-species, we noted that the initial
 428 increase in the pseudo-concentration of the DBE=10 compounds must be associated with
 429 hydrogenation of the abundant DBE=12 species (likewise, the hydrogenation of DBE=16
 430 compounds shifts them to the DBE=14 family). At higher conversion, two peaks were observed in
 431 the carbon number distributions, at 16 and 23 carbon atoms. Species with 16 carbon atoms could
 432 be bare carbazole structures with one hydrogenated ring. However, these species were also present
 433 in the effluents of VGO A and B and did not have particularly low reactivity. We, therefore, evoke
 434 the hypothesis that the two peaks could be derivatives of refractory species described in the work
 435 of Wiwel et al. [25]., i.e. carbazole species with an additional hepta-cycle (4,8,9,10-
 436 tetrahydrocyclohepta-[def]carbazole). The bare structure has 15 carbon atoms, an analogous
 437 structure with two additional naphthenic cycles of 23 carbon atoms.



438
 439 **Fig. 10.** The carbon number distributions of the carbazoles (DBE=10), benzocarbazoles (DBE=12
 440 and 14) and dibenzocarbazoles (DBE=16) in VGO C.

441 4.2.4. *Changes in carbon number distributions for HVGO VGO D*

442 In the case of VGO D, there was a fast consumption of less alkylated basic species below 35
443 carbon atoms (Fig. 7), similar to VGO A. For neutral N-species, the maximum of distribution
444 remained at 32 carbon atoms (Fig. 8).

445 Fig. A.10 illustrates that the lighter species, which were quickly converted, mainly belonged to
446 DBE=9 and DBE=11 families. Conversion above 35 carbon atoms was initially very low. The
447 intermediate accumulation of the DBE=7 and 8 species around 34 carbon atoms can be attributed
448 to the hydrogenation of higher DBE compounds and to the transfer of neutral nitrogen species
449 (mainly benzocarbazoles, as already suggested for VGO C).

450 As for the neutral nitrogen species, we observed an accumulation of lighter neutral nitrogen
451 species with DBE=10, which can be linked to the hydrogenation of benzocarbazoles with higher
452 DBEs (Fig. A.11). Similarly to VGO C, we observed a peak at 15 carbon atoms and its slow
453 conversion with increasing severity of conditions, which can be related to the presence of the
454 refractory structures as 4,8,9,10-tetrahydrocyclohepta-[def]carbazole. But it is difficult to explain
455 the nature of the accumulation of nC15 compounds at the beginning of hydrotreatment.

456

457 **5. Discussion**

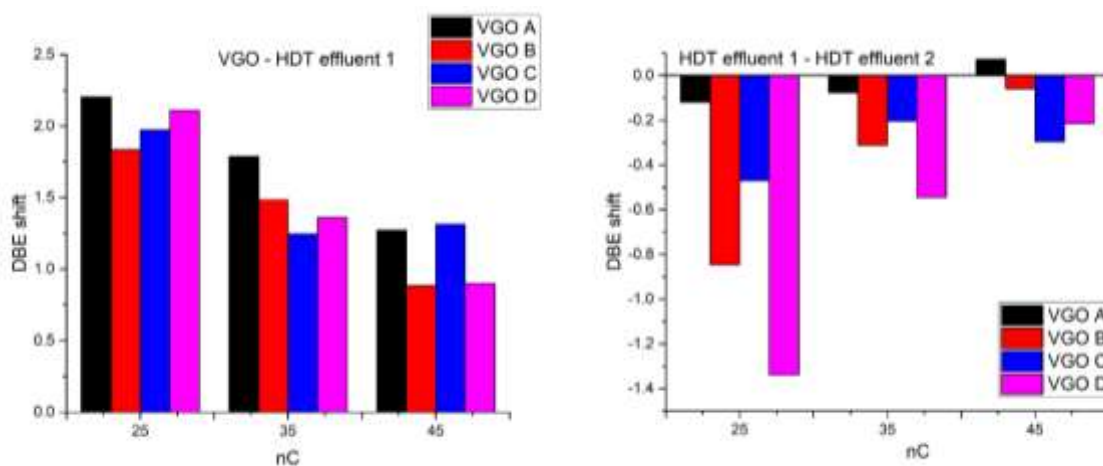
458 *5.1. Mechanisms of the VGO hydrodenitrogenation*

459 The previous two sections focused on the differences between the studied feeds in the HDN
460 process. Even though the analyzed feeds had different physicochemical properties and were of
461 different process origins, we can propose possible universal mechanisms for VGO HDN based on
462 the obtained DBE and carbon number distributions for each feed. Analyzing the behavior of the
463 basic nitrogen species within the degree of HDN conversion, one can conclude that the

464 transformation of quinolines with DBE=9 (or higher) into species with DBE=7 was common for
465 all feeds. For the two SR feeds A and B, this DBE shift largely explains the evolution of the basic
466 nitrogen species. Generally speaking, the hydrogenation of species with higher DBE (more than
467 DBE=8) is the source of production for the basic species with lower DBE. The hydrogenation of
468 a condensed aromatic ring generally leads to a -2 DBE shift; acridine species are an exception,
469 since the central ring is preferentially hydrogenated, which leads only to a -1 DBE shift [14]; a -3
470 DBE shift occurs in the case of hydrogenation of an isolated aromatic ring. Fig. 11 shows the
471 comparison of the weighted arithmetic mean DBE shift at the early hydrotreatment stage (the
472 difference between VGO and the first hydrotreated effluent produced at low HDN conversion) and
473 at the medium HDN stage (the difference between the first hydrotreated effluent obtained at low
474 HDN conversion and the medium HDN conversion effluent) at a fixed number of carbon atoms.
475 One can see that the reactions of hydrogenation of a condensed aromatic ring (-2 DBE shift) take
476 place at low and medium alkylation degrees (at 25 and 35 carbon atoms) for SR VGOs. Regarding
477 the medium HDN level, there was no dramatic change in DBE, or there even was a slight DBE
478 increase at low alkylation degree, since the hydrogenation stage has already been passed in most
479 species. We have also presented evidence that some of the basic species have been generated from
480 the transformation of neutral ones. Especially in the case of heavy coker gas oil VGO C, this leads
481 to very peculiar carbon number distributions in the effluents at intermediate HDN conversions.

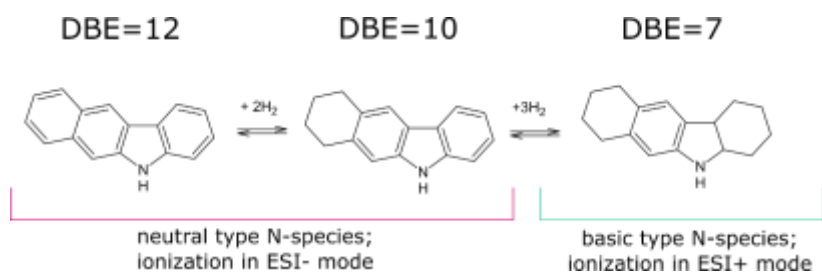
482 Returning to the transformation of neutral nitrogen species, we also observed the trend of
483 transformation of highly aromatic “source” species into species with lower DBE (and subsequent
484 hydrogenation into the basic N-species). At the beginning of hydrotreatment, for all four feeds, the
485 pseudo-concentration of species with DBE=10 was higher in the effluents than in the feeds as a
486 result of rapid hydrogenation of benzocarbazoles and dibenzocarbazoles. In the case of HCGO,

487 we observed that the accumulation of species with DBE=10 in the effluents was higher than in
488 other feeds. We relate it to the larger concentration of the carbazoles, dibenzocarbazoles, and the
489 presence of the fourth peak of benzonaphthocarbazoles in the feed. All these families are sources
490 for neutral N-species with DBE=10.



491
492 **Fig. 11.** The shift of the weighted arithmetic mean of DBE at the beginning of the
493 hydrotreatment (VGO – HDT effluent 1) and the medium HDN conversion (HDT effluent 1 –
494 HDT effluent 2).

495 An illustration of the mechanism of highly aromatic neutral species hydrogenation and
496 generation of basic ones is illustrated using benzocarbazole as an example in Fig. 12. In the first
497 step, hydrogenation of the side aromatic rings occurs, which leads to a shift to the left of the peaks
498 in the DBE distribution within the HDN level. After hydrogenation of the aromatic ring next to
499 the nitrogen-containing one, the character of the species becomes more basic, as the nitrogen
500 atom's lone pair of electrons is no more involved in aromatic bonds, and therefore it will be ionized
501 in positive ESI mode, and in the case of the illustrated example, we expect to see these species in
502 the distributions of the basics with DBE=7. These steps of rings hydrogenation are essential before
503 the subsequent cleavage of the C-N bond [39].



504
 505 **Fig. 12.** The hypothetical mechanism for hydrogenation of highly aromatic neutral nitrogen
 506 species and their transformation into the basic N-species.

507 The results also showed differences between the studied feeds. One of the most remarkable
 508 results was the different reactivity of the neutral N-species. The light neutral species were more
 509 reactive than the heavy ones in VGO A and VGO D, whereas in VGO B and C the opposite was
 510 the case. The carbon number distributions for the basic and neutral fractions were mostly smooth
 511 and monomodal in SR VGOs (except for a small peak at C20 for neutral high DBE compounds),
 512 while feeds C and D exhibited bimodal distributions in the neutral fraction. Taken together, these
 513 results suggest a higher presence of the compounds proposed in the work of Wiwel et al. [25] in
 514 the feeds issued from residue conversion. It is crucial to note that VGO C, which showed different
 515 behavior in the detailed carbon number distributions of nitrogen species, shows global kinetics
 516 similar to the SR VGO s. It can thus be conceivably hypothesized that the carbon number of N-
 517 species does not affect the global reactivity of the VGO during hydrotreatment. The lowest
 518 reactivity of the VGO D may be due to the fact that the neutral species, as carbazoles, that have
 519 been generated from heavy residuals, are more refractory. Fig. 6 shows that the amount of these
 520 carbazoles in VGO D is higher compared to other feeds.

521 5.2. Comparison to HDN of gas oils

522 Obviously, in gas oils, the nitrogen species have lower DBE and nC values, which is determined
 523 by the final boiling point of the fraction, which is lower in gas oils. In a study of Nguyen et al.

524 [20], a mixture of straight-run gas oil and coker gas oil (the boiling point at 95 % of yield is 397
525 °C) was characterized by the most abundant species with DBE=7-9 (quinolines family) and carbon
526 numbers C16-C24. In our case, the studied feeds also contain abundant species with the same DBE
527 values but with higher numbers of carbon atoms. The question arises if the behavior of VGO during
528 HDT will be similar to GO?

529 The following general trends were observed for the N1 basic nitrogen family during HDT. In
530 the case of the light fraction, the DBE of the basic species shifted to the left from DBE=8 to DBE=6
531 due to hydrogenation reactions (-2 DBE due to ring hydrogenation). In the case of VGO, a -2 DBE
532 shift of the DBE distribution maximum in the converted effluents was also observed (shift from
533 DBE=9 to DBE=7). Fig. A.12 demonstrates the changes in weighted arithmetic mean of DBE with
534 HDN in VGOs and a lighter fraction (GO) studied in the related work. Similar to the case of gas
535 oils, a high concentration of the low aromatic species as THQ Anilines Pyridines (DBE = 4-6) was
536 observed in the effluents at low and medium conversion HDN rates compared to the initial feed.

537 In contrast to basic compounds, neutral nitrogen compounds reacted differently in gas oils. In
538 the case of gas oils, the concentration of all neutral compounds reduced sharply with an increasing
539 degree of conversion compared to the VGO. At medium and high conversion rates, only small
540 amounts of carbazoles (DBE=9) and tetrahydrobenzocarbazoles (DBE=10) remained in the HDT
541 gas oil effluent, and their concentration remained approximately unchanged with the increasing
542 conversion rate. In the case of VGO, there was an increase in the concentration of carbazoles
543 (DBE=9-11) due to the conversion of species with higher DBE, such as benzocarbazoles,
544 dibenzocarbazoles, and benzonaphtocarbazoles, which are present in very low concentrations in
545 gas oils. We believe that the presence of these compounds led to a shift in the DBE distributions
546 in the case of VGO.

547 *5.3. Comparison to HDN of heavier fractions (residues)*

548 In contrast to DBE changes in hydrotreated VGO effluents, in the study of Li et al.[40], a slight
549 increase in DBE and alkylation degree of the basic nitrogen species within the hydrotreatment of
550 atmospheric residue (AR) was observed. The authors suggest that it happens due to the removal
551 of lighter molecules or (and) its condensation.

552 Neutral nitrogen components in the study of AR showed an increase in carbon number and a
553 decrease in DBE through hydrotreatment. An interesting point here is that similar to the case of
554 gas oils and VGOs (SR VGOs and HVGO), the DBE=10 was the most abundant in the most
555 hydrotreated AR effluent. Similar to VGO, the initial AR and effluents at the beginning of the
556 hydrotreatment had a high relative intensity of the dibenzocarbazoles (DBE=15), which probably
557 were converted into benzocarbazoles with DBE=12/13 and carbazoles with DBE=10 via
558 hydrogenation reactions.

559

560 **6. Conclusions**

561 Our study shows the differences in the N-species distributions at various HDN conversion
562 degrees in feeds of different process origins obtained by the (ESI+/-)-FTICR-MS. DBE vs. a
563 number of carbon atoms plots for two straight-run vacuum gas oils (SR VGO) characterized by
564 differences in macroscopic properties, as the content of the total nitrogen, density, and sulfur,
565 demonstrated similarities in the distribution of the most abundant peaks. The two feeds coming
566 from residue conversion processes, however, exhibited a distinctly different distribution of
567 nitrogen species, especially in the neutral fraction, which contained a high proportion of species
568 with very high DBE values.

569 By comparing the DBE/carbon number patterns of effluents with the feed, the reactivity of
570 species at specific DBE and carbon number values in the hydrotreating process can be figured out.
571 For heavy coker gas oil, the effect of the transition of neutral nitrogen species to basic during
572 hydrotreatment was clearly demonstrated. Also, for the other VGOs, neutral-to-basic N-species
573 transition processes probably occur, but kinetic modelling needs to be done to confirm them.

574 When comparing the results with lighter and heavier fractions, it was noted that the refractory
575 basic species are characterized by DBE=7 and DBE=8 (quinoline family). In the case of the
576 refractory neutral species, in all feeds, there were carbazoles with DBE=10. However, in the case
577 of VGO or heavier feeds compounds with DBE=12 and 13 remain also present in the effluents up
578 to very high HDN levels, due to hydrogenation of neutral species with higher DBE values which
579 are not present in gas oils.

580 In the discussion section, we have assumed that the carbon number of the species in the feed
581 does not affect the HDN reactivity of the VGO, as we saw by an example of the VGO C. At the
582 same time, we assumed that the low reactivity of the VGO D can be related to the more refractory
583 character of carbazoles generated from heavy residues. Additional study of the isomeric structures
584 of N-species probably will give an answer to the raised questions in this paper.

585 It is worth noting that a description of the reaction mechanisms and a selection of the versatile
586 reactivity descriptors of VGO HDT remains very complex due to the fact that the residual basic
587 and neutral N-containing structures are at the same time the result of the conversion of basic
588 and(or) neutral N-families, as well as the initial unconverted structures (due to refractory character
589 or due to competitive adsorption on the catalytic sites). At this level of data, we can observe only
590 the main trends and the differences within HDN intensity depending on the processing origin of
591 the VGOs. Understanding the structures of the selected species is still not possible at this level of

592 data, and it requires ion mobility and additional mass-spectrometry analyses, as the FTICR-MS
593 analysis does not provide information on isomeric content. Chemometric tools, supplementary
594 analytical data, and kinetic modelling will allow further interpretation of the data and a
595 determination of a key refractory species in VGO hydrotreatment.

596 **Appendices**

597 Simplified scheme of the pilot unit (**Fig. A.1**), comparison of the basic N1 families intensities in
598 the samples prepared with 0.5 mg/mL and 1 mg/mL of VGO (**Fig. A.2**), operating conditions and
599 physicochemical properties of the HDT effluents (**Table A.1**), description of the used analyses
600 (**Table A.2**), simulated distillation curves of vacuum gas oils (**Fig. A.3**), explanation of the
601 planar limit approach using the example of quinoline (**Fig. A.4**), the simple hypothetical
602 structures of the most abundant species in VGOs A-D (**Fig. A.5**), the carbon number
603 distributions of the quinolines (DBE=7-9) and acridines (DBE=11) in VGO A (**Fig. A.6**), the
604 carbon number distributions of the carbazoles (DBE=10), benzocarbazoles (DBE=12 and 14)
605 and dibenzocarbazoles (DBE=16) in VGO A (**Fig. A.7**), the carbon number distributions of the
606 quinolines (DBE=7-9) and acridines (DBE=11) in VGO B (**Fig. A.8**), the carbon number
607 distributions of the carbazoles (DBE=10), benzocarbazoles (DBE=12 and 14) and
608 dibenzocarbazoles (DBE=16) in VGO B (**Fig. A.9**), the carbon number distributions of the
609 quinolines (DBE=7-9) and acridines (DBE=11) in VGO D (**Fig. A.10**), the carbon number
610 distributions of the carbazoles (DBE=10), benzocarbazoles (DBE=12 and 14) and
611 dibenzocarbazoles (DBE=16) in VGO D (**Fig. A.11**), the weighted arithmetic mean of DBE as a
612 function of HDN in VGOs and gas oil (**Fig. A.12**).

613 **Acknowledgments**

614 This work was financially supported by IFP Energies Nouvelles and TotalEnergies, France.

- 616
617 [1] Girgis MJ, Gates BC. Reactivities, Reaction Networks, and Kinetics in High-pressure
618 Catalytic Hydroprocessing. *Ind. Eng. Chem. Res.* 1991;30(9):2021–58.
619 <https://doi.org/10.1021/ie00057a001>.
- 620 [2] Satterfield CN, Modell M, Wilkens JA. Simultaneous Catalytic Hydrodenitrogenation of
621 Pyridine and Hydrodesulfurization of Thiophene. *Ind. Eng. Chem. Process Des. Dev.*
622 1980;19(1):154–60. <https://doi.org/10.1021/i260073a027>.
- 623 [3] Sumbogo Murti SD, Yang H, Choi K-H, Korai Y, Mochida I. Influences of Nitrogen
624 Species on the Hydrodesulfurization Reactivity of a Gas Oil Over Sulfide Catalysts of
625 Variable Activity. *Applied Catalysis A: General* 2003;252(2):331–46.
626 [https://doi.org/10.1016/S0926-860X\(03\)00468-X](https://doi.org/10.1016/S0926-860X(03)00468-X).
- 627 [4] Zeuthen P, Schmidt M, Rasmussen HW, Moyses BM. The benefits of cat feed hydrotreating
628 and the impact of feed nitrogen on catalyst stability. *NPRA Annual Meeting Technical*
629 *Papers* 2010;2:818–33.
- 630 [5] Stratiev D, Shishkova I, Ivanov M, Dinkov R, Georgiev B, Argirov G et al. Catalytic
631 Cracking of Diverse Vacuum Residue Hydrocracking Gas Oils. *Chem Eng & Technol*
632 2021;44(6):997–1008. <https://doi.org/10.1002/ceat.202000577>.
- 633 [6] Vistisen PØ, Zeuthen P. Reactions of Organic Sulfur and Nitrogen Compounds in the FCC
634 Pretreater and the FCC Unit. *Ind. Eng. Chem. Res.* 2008;47(21):8471–7.
635 <https://doi.org/10.1021/ie8006616>.
- 636 [7] McIlvried HG. Kinetics of the Hydrodenitrification of Pyridine. *Ind. Eng. Chem. Process*
637 *Des. Dev.* 1971;10:125–30. <https://doi.org/10.1021/i260037a023>.
- 638 [8] Raghuvver CS, Thybaut JW, Bruycker R de, Metaxas K, Bera T, Marin GB. Pyridine
639 Hydrodenitrogenation Over Industrial NiMo/ γ -Al₂O₃ Catalyst: Application of Gas Phase
640 Kinetic Models to Liquid Phase Reactions. *Fuel* 2014;125:206–18.
641 <https://doi.org/10.1016/j.fuel.2014.02.017>.
- 642 [9] Pille R, Froment G. Kinetic Study of the Hydrodenitrogenation of Pyridine and Piperidine
643 on a NiMo Catalyst. *Studies in Surface Science and Catalysis* 1997;106:403–13.
644 [https://doi.org/10.1016/S0167-2991\(97\)80038-9](https://doi.org/10.1016/S0167-2991(97)80038-9).
- 645 [10] Nguyen M-T, Tayakout-Fayolle M, Pirngruber GD, Chainet F, Geantet C. Kinetic Modeling
646 of Quinoline Hydrodenitrogenation over a NiMo(P)/Al₂O₃ Catalyst in a Batch Reactor. *Ind.*
647 *Eng. Chem. Res.* 2015;54(38):9278–88. <https://doi.org/10.1021/acs.iecr.5b02175>.
- 648 [11] Satterfield CN, Cocchetto JF. Reaction Network and Kinetics of the Vapor-Phase Catalytic
649 Hydrodenitrogenation of Quinoline. *Ind. Eng. Chem. Process Des. Dev.* 1981;20(1):53–62.
650 <https://doi.org/10.1021/i200012a008>.
- 651 [12] Yang SH, Satterfield CN. Catalytic Hydrodenitrogenation of Quinoline in a Trickle-Bed
652 Reactor. Effect of Hydrogen Sulfide. *Ind. Eng. Chem. Process Des. Dev.* 1984;23(1):20–5.
653 <https://doi.org/10.1021/i200024a003>.
- 654 [13] Prins R, Jian M, Flechsenhar M. Mechanism and Kinetics of Hydrodenitrogenation.
655 *Polyhedron* 1997;16(18):3235–46. [https://doi.org/10.1016/S0277-5387\(97\)00111-3](https://doi.org/10.1016/S0277-5387(97)00111-3).
- 656 [14] Rabarihoela-Rakotovo V, Diehl F, Brunet S. Deep HDS of Diesel Fuel: Inhibiting Effect of
657 Nitrogen Compounds on the Transformation of the Refractory 4,6-
658 Dimethyldibenzothiophene Over a NiMoP/Al₂O₃ Catalyst. *Catal Lett* 2009;129(1-2):50–60.
659 <https://doi.org/10.1007/s10562-008-9777-x>.

- 660 [15] Bunch A, Zhang L, Karakas G, Ozkan US. Reaction Network of Indole
661 Hydrodenitrogenation over NiMoS/ γ -Al₂O₃ Catalysts. *Applied Catalysis A: General*
662 2000;190(1-2):51–60. [https://doi.org/10.1016/S0926-860X\(99\)00270-7](https://doi.org/10.1016/S0926-860X(99)00270-7).
- 663 [16] Kim SC, Massoth FE. Kinetics of the Hydrodenitrogenation of Indole. *Ind. Eng. Chem. Res.*
664 2000;39(6):1705–12. <https://doi.org/10.1021/ie9906518>.
- 665 [17] Nguyen M-T, Pirngruber GD, Chainet F, Tayakout-Fayolle M, Geantet C. Indole
666 Hydrodenitrogenation over Alumina and Silica–Alumina-Supported Sulfide Catalysts—
667 Comparison with Quinoline. *Ind. Eng. Chem. Res.* 2017;56(39):11088–99.
668 <https://doi.org/10.1021/acs.iecr.7b02993>.
- 669 [18] Boduszynski MM. Composition of Heavy Petroleum. 2. Molecular Characterization.
670 *Energy Fuels* 1988;2(5):597–613. <https://doi.org/10.1021/ef00011a001>.
- 671 [19] Shin S, Sakanishi K, Mochida I, Grudowski DA, Shinn JH. Identification and Reactivity of
672 Nitrogen Molecular Species in Gas Oils. *Energy Fuels* 2000;14(3):539–44.
673 <https://doi.org/10.1021/ef990136m>.
- 674 [20] Nguyen M-T, Pirngruber GD, Chainet F, Albrieux F, Tayakout-Fayolle M, Geantet C.
675 Molecular-Level Insights into Coker/Straight-Run Gas Oil Hydrodenitrogenation by Fourier
676 Transform Ion Cyclotron Resonance Mass Spectrometry. *Energy Fuels* 2019;33(4):3034–
677 46. <https://doi.org/10.1021/acs.energyfuels.8b04432>.
- 678 [21] Le Maître J, Hubert-Roux M, Paupy B, Marceau S, Rüger CP, Afonso C et al. Structural
679 Analysis of Heavy Oil Fractions After Hydrodenitrogenation by High-Resolution Tandem
680 Mass Spectrometry and Ion Mobility Spectrometry. *Faraday Discuss* 2019;218:417–30.
681 <https://doi.org/10.1039/C8FD00239H>.
- 682 [22] Le Maître J, Paupy B, Hubert-Roux M, Marceau S, Rüger C, Afonso C et al. Structural
683 Analysis of Neutral Nitrogen Compounds Refractory to the Hydrodenitrogenation Process
684 of Heavy Oil Fractions by High-Resolution Tandem Mass Spectrometry and Ion Mobility–
685 Mass Spectrometry. *Energy Fuels* 2020;34(8):9328–38.
686 <https://doi.org/10.1021/acs.energyfuels.0c01160>.
- 687 [23] Wen S-C, Zhou Y-S, Wei Q. Hydrogenation Performance of Nitrogen Containing
688 Compounds Present in Coker Gas Oil. *Acta Petrolei Sinica (Petroleum Processing Section)*
689 2008, 2008:496–502.
- 690 [24] Guillemant J, Berlioz-Barbier A, Oliveira LP de, Albrieux F, Lacoue-Nègre M, Duponchel
691 L et al. Exploration of the Reactivity of Heteroatomic Compounds Contained in Vacuum
692 Gas Oils during Hydrotreatment Using Fourier Transform Ion Cyclotron Resonance Mass
693 Spectrometry. *Energy Fuels* 2020;34(9):10752–61.
694 <https://doi.org/10.1021/acs.energyfuels.0c01760>.
- 695 [25] Wiwel P, Hinnemann B, Hidalgo-Vivas A, Zeuthen P, Petersen BO, Duus JØ.
696 Characterization and Identification of the most Refractory Nitrogen Compounds in
697 Hydroprocessed Vacuum Gas Oil. *Ind. Eng. Chem. Res.* 2010;49(7):3184–93.
698 <https://doi.org/10.1021/ie901473x>.
- 699 [26] Celis-Cornejo CM, Pérez-Martínez DJ, Orrego-Ruiz JA, Baldovino-Medrano VG.
700 Identification of Refractory Weakly Basic Nitrogen Compounds in a Deeply Hydrotreated
701 Vacuum Gas Oil and Assessment of the Effect of Some Representative Species over the
702 Performance of a Ni–MoS₂/Y-Zeolite–Alumina Catalyst in Phenanthrene Hydrocracking.
703 *Energy Fuels* 2018;32(8):8715–26. <https://doi.org/10.1021/acs.energyfuels.8b02045>.
- 704 [27] Merdignac I. Composition des Structures Azotées dans les Pétroles. Implication pour leur
705 Réactivité au cours des Procédés d’Hydrodésazotation. Université Louis Pasteur; 1997.

- 706 [28] Manek E, Haydary J. Hydrocracking of Vacuum Residue with Solid and Dispersed Phase
707 Catalyst: Modeling of Sediment Formation and Hydrodesulfurization. *Fuel Processing*
708 *Technology* 2017;159:320–7. <https://doi.org/10.1016/j.fuproc.2017.02.003>.
- 709 [29] Sahu R, Song BJ, Im JS, Jeon Y-P, Lee CW. A Review of Recent Advances in Catalytic
710 Hydrocracking of Heavy Residues. *Journal of Industrial and Engineering Chemistry*
711 2015;27:12–24. <https://doi.org/10.1016/j.jiec.2015.01.011>.
- 712 [30] Meyers RA. *Handbook of petroleum refining processes*. 4th ed. New York NY: McGraw-
713 Hill Education; 2016.
- 714 [31] Purcell JM, Rodgers RP, Hendrickson CL, Marshall AG. Speciation of Nitrogen Containing
715 Aromatics by Atmospheric Pressure Photoionization or Electrospray Ionization Fourier
716 Transform Ion Cyclotron Resonance Mass Spectrometry. *J Am Soc Mass Spectrom*
717 2007;18(7):1265–73. <https://doi.org/10.1016/j.jasms.2007.03.030>.
- 718 [32] Charon-Revellin N, Dulot H, López-García C, Jose J. Kinetic Modeling of Vacuum Gas Oil
719 Hydrotreatment using a Molecular Reconstruction Approach. *Oil Gas Sci. Technol. – Rev.*
720 *IFP Energies nouvelles* 2011;66(3):479–90. <https://doi.org/10.2516/ogst/2010005>.
- 721 [33] Klein GC, Rodgers RP, Marshall AG. Identification of Hydrotreatment-Resistant
722 Heteroatomic Species in a Crude Oil Distillation Cut by Electrospray Ionization FT-ICR
723 Mass Spectrometry. *Fuel* 2006;85(14-15):2071–80.
724 <https://doi.org/10.1016/j.fuel.2006.04.004>.
- 725 [34] Mullins OC, Sheu EY, Hammami A, Marshall AG (eds.). *Asphaltenes, heavy oils, and*
726 *petroleomics*. New York: Springer; 2007.
- 727 [35] Guillemant J, Albrieux F, Oliveira LP de, Lacoue-Nègre M, Duponchel L, Joly J-F. Insights
728 from Nitrogen Compounds in Gas Oils Highlighted by High-Resolution Fourier Transform
729 Mass Spectrometry. *Anal Chem* 2019;91(20):12644–52.
730 <https://doi.org/10.1021/acs.analchem.9b01702>.
- 731 [36] Guillemant J, Albrieux F, Lacoue-Nègre M, Pereira de Oliveira L, Joly J-F, Duponchel L.
732 Chemometric Exploration of APPI(+)-FT-ICR MS Data Sets for a Comprehensive Study of
733 Aromatic Sulfur Compounds in Gas Oils. *Anal Chem* 2019;91(18):11785–93.
734 <https://doi.org/10.1021/acs.analchem.9b02409>.
- 735 [37] Cho Y, Kim YH, Kim S. Planar Limit-Assisted Structural Interpretation of
736 Saturates/Aromatics/Resins/Asphaltenes Fractionated Crude Oil Compounds Observed by
737 Fourier Transform Ion Cyclotron Resonance Mass Spectrometry. *Anal Chem*
738 2011;83(15):6068–73. <https://doi.org/10.1021/ac2011685>.
- 739 [38] Nagai M, Masunaga T, Hanaoka N. Hydrodenitrogenation of Carbazole on a Mo/Al₂O₃
740 Catalyst. Effects of Sulfiding and Sulfur Compounds. *Energy Fuels* 1988;2(5):645–51.
741 <https://doi.org/10.1021/ef00011a007>.
- 742 [39] Tominaga H, Nagai M. Reaction mechanism for hydrodenitrogenation of carbazole on
743 molybdenum nitride based on DFT study. *Applied Catalysis A: General* 2010;389(1-2):195–
744 204. <https://doi.org/10.1016/j.apcata.2010.09.020>.
- 745 [40] Li Y-E, Guan Y-M, Liu M, Yuan S-H, Zhang C, Song Y-Y. Transformation of Basic and
746 Non-basic Nitrogen Compounds during Heavy Oil Hydrotreating on Two Typical Catalyst
747 Gradations. *Energy Fuels* 2021;35(3):2826–37.
748 <https://doi.org/10.1021/acs.energyfuels.0c03028>.